ACS ES&T Water

pubs.acs.org/estwater

Article

Engineering Novel Thin-Film Composite Membrane for Efficient Forward Osmosis Desalination: Fabrication and Performance Evaluation

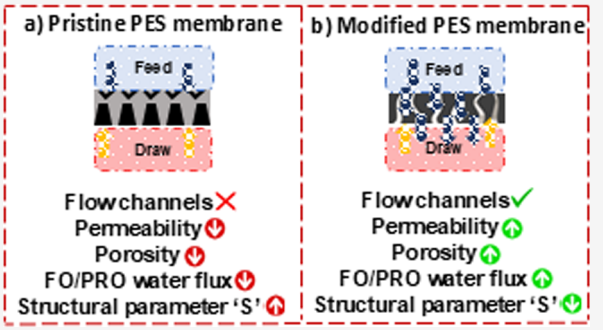
Shubham Ketan Sharma and Bhaskar Jyoti Deka*

Cite This: ACS EST Water 2024, 4, 5913−5924

Read Online

ACCESS | Metrics & More | Article Recommendations | Supporting Information

ABSTRACT: Forward osmosis (FO) represents an innovative avenue for energy-efficient water generation from a saline feed. This work presents the development of a thin-film composite (TFC) FO membrane for desalination application. The membrane support layer was fabricated using polyether sulfone (PES) and was modified with poly(2-ethyl-2-oxazoline) (PEOx) and goethite nanoparticles as hydrophilic enhancers. The peak occurring at 1637 cm^{-1} in FTIR spectra confirmed the presence of PEOx. Moreover, X-ray diffraction spectra of the membrane substrate displayed distinct peaks at 21.40, 33.53, 34.8, and 36.73°, indicative of the presence of geothite nanoparticles. The morphologies of fabricated PES support layers were observed to be significantly porous in scanning electron microscopy images, along with improved porosity and average pore size. The support layer achieved a superhydrophilic loose side (∼0° WCA) and a hydrophilic dense side (∼50.7° WCA), indicating enhanced wetting characteristics. Additionally, the support layer demonstrated the development of a selective polyamide layer. The water permeability coefficient "A" of the TFC-FO membrane was enhanced, and the structural parameter "S" was reduced dramatically. Furthermore, the optimal membrane TFC-M4 exhibited nearly 5.62 and 11.25 LMH flux under FO and PRO modes respectively, with 2 M NaCl draw and deionized water as feed solutions.



KEYWORDS: *Poly(oxazoline), goethite, hydrophilicity, forward osmosis, poly(ether sulfone), nanoparticles*

1. INTRODUCTION

The increased demand for freshwater resources is now recognized as a strategic necessity, resulting due to the fast expansion of the human population and economy. This eventually results in the consumption of vital natural assets.[1] Researchers are making efforts across the globe to augment freshwater resources. Desalination technology for seawater represents a crucial strategic means of addressing the pressing global water scarcity challenges, hence offering significant potential and essential utility.[2] Over the past few years, forward osmosis (FO) has acknowledged recognition as an energy-efficient technology.[3−6] The operation of this process relies on osmotic pressure differentials arising from the lower osmotic pressure occurring at the feed and the higher osmotic pressure occurring at the draw side. This gradient propels the water flow through the FO membrane. Compared to pressure-based desalination technologies, FO holds several advantages, including reduced energy consumption, increased water recovery rates, and lowered equipment costs.[7−10] Developing high-performance FO membranes stands as a focal point of research in the field of FO. An optimal FO membrane must exhibit higher water flux while effectively limiting reverse salt flux throughout the process of FO.[11] Typically, these membranes can be classified in three major kinds, which involve (i) membranes constructed through a layer-by-layer concept, (ii) asymmetric membranes, and (iii) thin-film composite (TFC) membranes.[12−15] TFC membranes have received constructive responses from researchers, as they exhibit superior FO performance and have wide pH applicability. These membranes feature a porous substrate that supports a very thin active layer.[16] This support layer in FO membranes enhances structural integrity and stability and supports the attachment of the active layer, crucial for optimizing membrane performance. Consequently, the primary focus of researchers in TFC FO membrane studies lies in developing optimal support substrates.

Amidst their array of benefits, TFC FO membranes are hampered by a formidable challenge, known as internal concentration polarization (ICP). ICP arises from the barrier to diffusion within FO membranes, hence declining the

Received: September 12, 2024
Revised: November 27, 2024
Accepted: November 27, 2024
Published: December 4, 2024



Downloaded from pubs.acs.org/aewcaa/article-pdf/4/12/5913/3163023/ew4c00877.pdf by DOKUZ EYLUL UNIV user on 02 September 2026

© 2024 American Chemical Society

https://doi.org/10.1021/acsestwater.4c00877
ACS EST Water 2024, 4, 5913−5924

osmotic pressure through the membrane.[17] ICP is inherent to FO membranes that reside within the porous substrate and cannot be addressed by hydrodynamic optimization. This, in turn, makes membrane fabrication optimization crucial for ICP mitigation. Researchers have made numerous efforts to mitigate the adverse effects of ICP while aiming for enhanced permeability of FO membranes. Optimizing membrane structure is an efficient pathway to decrease ICP and enhance FO performance.[18] In this reference, Shokrollahzadeh and Tajik designed an electrospun polyacrylonitrile nanofiber membrane with a unique structure, lower tortuosity, and high porosity to address ICP.[19] However, the electrospinning technique presents a costly and intricate hurdle for large-scale manufacturing. One of the research investigations for mitigating ICP involved modifying the PSf substrate by adding sulfonated phenylene oxide. This modification leads to a substantial enhancement in membrane performance due to enhanced wettability. However, PSf is susceptible to hydrolysis under specific conditions, potentially diminishing its strength and performance during prolonged working hours. Polymers, such as polyether sulfone (PES) and polyvinylidene fluoride, stand out as primary backbone polymers for fabricating TFC FO membrane substrates.[20,21] PES exhibits exceptional thermal and chemical resistance, along with hydrolytic and mechanical stability properties. However, these polymers have an inherent hydrophobic nature. The inherent hydrophobicity hinders complete pore wetting, leading to fewer effective substrate areas for mass transport. Hence, enhancing the hydrophilicity of these polymers to fabricate a substrate matrix for FO membranes becomes imperative to mitigate ICP.

In recent times, a multitude of methods, encompassing both physical and chemical alterations, have been employed for enhancing the hydrophilicity of membrane substrates containing PES. Incorporating hydrophilic nanoparticles (NPs) into substrates represents a viable strategy. Bagherzadeh et al. research explored the use of MOF-modified polyamide layers, utilizing WS_2−Cys-UiO-66$(CO_2H)_2$.[22] Incorporating WS_2−Cys-MOF (compatible with polymer matrix) into the PA layer resulted in a smooth surface with defect-free channels, enhancing water flux and resistance to fouling in the TFN membrane. Additionally, the angstrom-sized pores of the MOF resulted in selective transfer and separation of ions. Sirinupong et al. introduced TiO_2 NPs into the PES substrates, resulting in better hydrophilicity and porosity.[23] This, in turn, reduced the ICP. Some studies have also utilized sulfonated polymers as additives to prepare the substrate. Their strategy involves the sulfonation of the PES to confer the hydrophilic properties onto the polymer.[24] However, the dimensional stability in aqueous solutions might become problematic with higher concentrations of sulfonated materials in the membrane. Furthermore, the widely employed additives and modifiers are expensive and less environmentally benign. Therefore, emphasis should be placed on developing approaches that employ novel, environmentally sustainable, and cost-effective methods for fabricating membranes suitable for FO applications.

Poly(2-ethyl-2-oxazoline) (PEOx) emerges as a water-soluble and biocompatible polymer with temperature- and pH-responsive characteristics.[25] Its biocompatibility presents it as promising for diverse biomedical applications including drug delivery, imaging, and tissue regeneration.[26,27] PEOx is abundant in hydrogen bonding sites due to the presence of the (−C(O)−N−) bond that makes it readily interact with water. It has superior hygroscopicity, surpassing that of polyethylene glycol (PEG) and polyvinylene pyrrolidone (PVP), this makes PEOx suitable for enhancing hydrophilicity when incorporated into the polymer matrix.[28] Observations indicate that including a hydrophilic additive can effectively enhance the wetting characteristics of the membrane substrate. Hence, adding PEOx as a hydrophilic modifier can be a competitive hydrophilic modifier for preparing membrane support substrates for TFC-FO membranes.

To enhance overall membrane performance, it is critical to improve the water contact angle (CA), specifically on the dense side of the membrane. Introducing hydrophilic NPs serves as a viable approach to achieve this enhancement. During the membrane development process through non-solvent-induced phase separation, these NPs exhibit migration toward the surface, thereby amplifying the hydrophilic properties of the dense side. In this respect, iron-oxide-based NPs, notably Goethite NPs (Goe NPs), offer hydrophilic and biocompatible properties. Goethite is an iron oxyhydroxide that has an orthorhombic crystal structure and is yellowish in color. The surface of Goe NPs is characterized by the presence of hydroxyl groups.[29] Incorporating these NPs in the membrane support substrate for developing the TFC FO membrane can be a potential approach to improve membrane hydrophilicity on the dense side of the support substrates. However, exceeding a limiting concentration of these NPs leads to agglomeration and hence limits its application in enhancing the hydrophilicity.[30]

This study presents a novel attempt at fabricating an advanced TFC FO membrane with superior performance and lower development costs. Hence, PES was picked as a moderate-cost base polymer, and PEOx and Goe NPs were used as hydrophilic additives to prepare the support substrate for the fabrication of the TFC FO membrane. The performance and characteristics of the membrane substrates were investigated by utilizing different studies, including morphological analysis, water CA, and porosity analysis, Fourier transform infrared (FTIR), and X-ray diffraction (XRD) studies. Furthermore, the influence of the substrates on the microstructure and fundamental characteristics of the TFC FO membranes were explored. Lastly, an ideal membrane was decided on the basis of the FO performance and intrinsic properties obtained for the TFC FO membranes.

2. MATERIALS AND METHODS

2.1. Materials. Polyether sulfone (M_w, 55,000), PEOx (M_w, 50,000), and Goe NPs (M_w, 88.85) were employed for the preparation of the membrane substrate. Dimethylacetamide was used as the solvent to prepare the membrane substrate. Trimesoyl chloride (TMC, >99%, Sigma-Aldrich), *M*-phenylenediamine (MPD, >98%, Sigma-Aldrich), and *n*-hexane (>95%) were employed for the process of interfacial polymerization (IP). Sodium chloride (NaCl, >99.5%) was utilized as the draw solution agent.

2.2. Creation of TFC-FO Membrane. *2.2.1. Substrate Formation via Phase Inversion.* The PES/PEOx/Goe substrates were developed utilizing the nonsolvent-induced phase separation process, refer to Figure S1. The casting solutions and their compositions are listed in Table 1. The Goe NPs (0.5 wt %, concentration) were sonicated for 10−15 min in the DMAc solvent. The concentration of Goe NPs was decided based on the AFM results; refer to Figure S2 and Table S1. Later on, the particular amounts of PES and PEOx

Downloaded from pubs.acs.org/aewcaa/article-pdf/4/12/5913/3163023/ew4c00877.pdf by DOKUZ EYLUL UNIV user on 02 September 2026

https://doi.org/10.1021/acsestwater.4c00877
ACS EST Water 2024, 4, 5913−5924

Table 1. Formulations of the Diverse Casting Solutions for Preparing the Substrate

	polymer		NP	solvent
membranes	PES (wt %)	PEOx (wt %)	goethite (wt %)	DMAc (wt %)
M0	12	0	0	88
M2	12	2	0.5	85.5
M4	12	4	0.5	83.5
M6	12	6	0.5	81.5

were stirred and dissolved in solution continuously at 60 °C for 10 h to obtain a homogeneous solution. Furthermore, this homogeneous polymer solution was applied on a glass plate by means of a casting knife, ensuring a consistent distance of 250 μm. The casted membrane substrates were submerged in water (coagulant medium) to complete the phase separation process. The membranes were removed from the water upon the detachment from the glass plate. Subsequently, the acquired substrates were transmitted into a water bath for eliminating the residual solvent under the flowing water.

2.2.2. Selective Layer Preparation via IP. The active layer was developed by polymerizing TMC and MPD monomers over the PES/PEOx/Goe substrate; refer to Figure S3. This results in the formation of polyamide over the membrane surface. Initially, the prepared substrates were incubated in an aqueous solution of MPD (3.4 wt %) for a time period of 2 min. Subsequently, surplus MPD solution was recovered utilizing filter paper and a rubber roller. Following this, a TMC solution (0.1 wt %) was carefully applied for 60 s onto the surface of the MPD-soaked substrate. Upon draining the excess TMC solution, the nascent TFC membranes underwent oven curing for 10 min at 70 °C. The resulting TFC membranes were washed to eliminate the remaining monomers. Further, these membranes were stored in distilled water for characterization and performance analysis. Based on the substrate labels, these membranes were labeled TFC-M0, TFC-M2, TFC-M4, and TFC-M6.

2.3. Membrane Characterization. *2.3.1. Microstructure of the Substrates and Active Layer.* The substrate and active layer were examined for their microstructure using a scanning electron microscope (Carl-Zeiss Ultra Plus field-emission scanning electron microscope). The membrane samples were initially dried for 48 h. Following this, the samples were gold-coated by using a sputtering coater. To analyze and observe the cross section, the prepared samples were flash-frozen and cracked utilizing cryogenic nitrogen before undergoing drying followed by scanning electron microscopy (SEM) analysis.

2.3.2. Characterization of Substrates. The substrate porosity (ε) was determined by calculating the variation between the sample's wet and dry weights as mentioned in eq 1, where m_1, m_2, ρ_m, and ρ_i represent the wet weight, dry weight, density of the polymer, and density of wetting solvent, respectively.

$$\varepsilon = \frac{\left(\frac{m_1 - m_2}{\rho_i}\right)}{\frac{(m_1 - m_2)}{\rho_i} + \left(\frac{m_2}{\rho_m}\right)} \tag{1}$$

The pore size avg (r_m) was measured after using the porosity and pure water permeability data and applying in the Guerout–Elford–Ferry equation as mentioned in eq 2, where T and η relate to the thickness of the substrates and deionized (DI) water viscosity, respectively.

$$r_m = \sqrt{\frac{8 \times (2.9 - 1.75\varepsilon) \times T \times \eta \times PWP}{\varepsilon}} \tag{2}$$

The measurement of the CA of substrates was assessed by utilizing a drop shape analyzer (model: Kruss DSA 25B). Around 2 μL of DI water was dispensed onto a substrate surface (dried) for testing. Images were promptly captured upon the water droplets coming into contact with the substrate surface. Around 5 measurements were conducted at arbitrary locations on each sample, and an average value is reported.

The comprehensive characterization of the membrane samples to determine various functional groups was conducted through FTIR analysis. Furthermore, XRD and energy-dispersive X-ray (EDX), along with X-ray photoelectron spectroscopy (XPS) were performed to ascertain the membrane crystallinity and to validate the presence of Goe NPs embedded within the membrane structure.

2.3.3. Intrinsic Properties of the TFC Membrane. The values of the permeability of water (A) and salt permeability (B) were evaluated in the RO testing mode. The A value was determined by running the membrane substrate in the RO mode at 5.0 bar pressure using DI water as the feed. The value of A was measured employing eq 3, where ΔV_a relates to the volume of the permeate for a fixed time Δt_a. Additionally, A_m is related to the effective area of the TFC membrane and ΔP is related to the transmembrane pressure difference.

$$A = \frac{\Delta V_a}{\Delta t_a \times A_m \times \Delta P} \tag{3}$$

Salt permeability (B) was determined through salt rejection (R_s) calculations and using the A value.[31] The value of R_s was obtained utilizing 2 M NaCl solution as feed and subjecting it to a pressure of 1.0 bar. Equations 4 and (5) were utilized to calculate R_s and B values, respectively, where C_f and C_p represent the NaCl concentration of the feed and permeate solutions, respectively, while ΔP and $\Delta\pi$ denote the trans-membrane hydraulic and osmotic pressure differences, respectively.

$$R_s = \frac{C_f - C_p}{C_f} \times 100\% \tag{4}$$

$$B = A \times \left\{\frac{1}{R_s} - 1\right\} \times (\Delta P - \Delta\pi) \tag{5}$$

The method of classical flux-fitting was employed to measure the structural parameter (S) utilizing the equation given in eq 6, where D denotes the coefficient of solute diffusion and π_{draw} and π_{feed} represent the draw side and feed side osmotic pressures, respectively.[32] J_w represents the water flux obtained for the FO mode in the performance tests.

$$S = \frac{D}{J_w}\left[\ln \frac{A \times \pi_{draw} + B}{A \times \pi_{feed} + J_w + B}\right] \tag{6}$$

2.4. Evaluation of FO Performance. The performance of FO was assessed using the laboratory-scale cross-flow filtration system featuring a membrane area of 3 × 8 cm's (refer to Figure S4). The solutions (feed and draw) were circulated concurrently at a constant cross-flow rate of 200–300 mL/

Downloaded from pubs.acs.org/aewcaa/article-pdf/4/12/5913/3163023/ew4c00877.pdf by DOKUZ EYLUL UNIV user on 02 September 2026

https://doi.org/10.1021/acsestwater.4c00877
ACS EST Water 2024, 4, 5913–5924

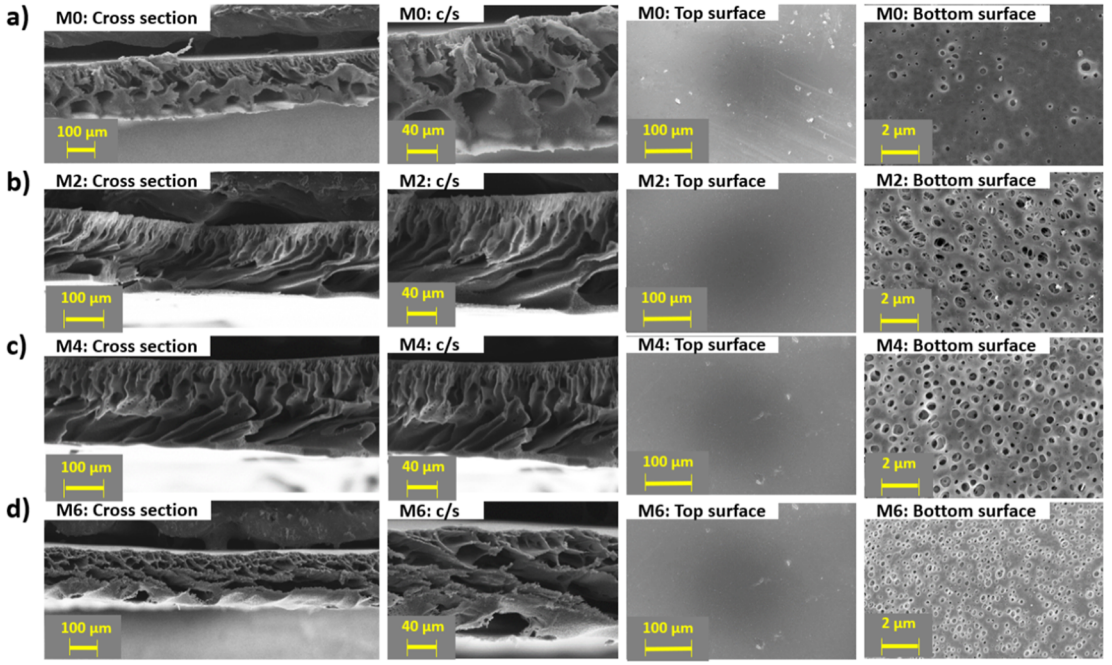


Figure 1. Morphological images illustrating diverse membrane support layers, representing cross section (at 500× and 1000× magnification), top surfaces (at 200× magnification), and bottom surfaces (at 10 K × magnification) of (a) M0 membrane representing pristine PES membrane, (b) M2 membrane with 2 wt % PEOx, (c) M4 membrane with 4 wt % PEOx, and (d) M6 membrane with 6 wt % PEOx.

min. DI water was utilized as feed while NaCl was the draw solution. To measure water flux (J_w), the changes in the weight of the NaCl solution were monitored by using a data-logging system while the reverse salt flux (J_s) was examined by tracking changes in the concentration of NaCl in the feed solution with a conductivity meter. All FO performance assessments were conducted over a period of 5 h, with J_w and J_s values calculated for 10 min intervals. Two operational modes were investigated: FO mode (with the active layer facing the feed side) and pressure-retarded osmosis (PRO) mode (with the active layer facing the draw side).

The values of J_w and J_s were computed using eqs 7 and 8, wherein ΔV denotes the variation in the draw solution's volume over a fixed time interval Δt and S_m denotes the effective area of the TFC membrane. C_t and C_o indicate the final and initial concentrations of salt in the feed solution, respectively. V_t and V_o represent the final and initial volumes of the feed solution, respectively.

$$J_w = \frac{\Delta V}{S_m \times \Delta t} \tag{7}$$

$$J_s = \frac{C_t \times V_t - C_o \times V_o}{S_m \times \Delta t} \tag{8}$$

3. RESULTS AND DISCUSSION

3.1. Properties and Performance of the Substrates.

3.1.1. Morphology of the Substrates. Multiple paths can be followed during the phase inversion stage by the initial solution of the polymer. This can be elucidated utilizing a ternary diagram.[33] As per the ternary diagram, the instantaneous demixing promotes macro-void formation. Figure 1 shows the FESEM images for the top and bottom surface and the cross section of the membrane substrates. All membranes demonstrated an asymmetric membrane structure characterized by a dense top layer and porous sublayer. At the same time, EDX spectroscopy (EDS) analysis confirmed the presence of Goe NPs in the composite substrates, as shown in Figure S5. The results indicated that the goethite is evenly dispersed in the substrates compared to the pristine PES membrane substrate. An increase in the oxygen content in EDS for the membrane modified with the Goe NPs reflects the incorporation of the NPs, and the peak of the hydroxyl groups in the XPS analysis also confirms the presence of goethite, refer to Figure S6.

The substrates fabricated from pristine PES showcased macro-voids dispersed throughout the majority of sections, accompanied by a thin finger-like layer adjacent to the top surface. The formation of macro-voids is ascribed to the reduced polymer phase concentration within the sublayer, allowing ample time for the nonsolvent to initiate nucleation and subsequent growth.[34] A rise in the PEOx concentration within the casting solution relates with an augmentation in the formation of finger-like pores within the sublayer, consequently yielding membranes with increased porosity. The pores began to interconnect, primarily toward the lower section of the substrates, for the M2 and M4 membranes. According to Smolders theory, this phenomenon is primarily ascribed to the inherently hydrophilic character of additives, which greatly enhances the rate of diffusion during phase separation.[35] This, therefore, augments the thermodynamic instability within the casting solution. Hence, the exchange rate between the solvent and nonsolvent effectively augmented and enhanced during the process of phase separation. A similar phenomenon was found in Wang's research.[36] This indicates that PEOx contributes positively to enhancing the substrate's porosity. However, an irregularity becomes apparent in the finger-like layer in the sublayer when the concentration of PEOx increases to 6 wt %. This can be due to the increased polymer concentration that encourages polymer aggregation, forming larger polymer domains within the membrane. Additionally, higher polymer concentrations can elevate the viscosity of the polymer

Downloaded from pubs.acs.org/aewcaa/article-pdf/4/12/5913/3163023/ew4c00877.pdf by DOKUZ EYLUL UNIV user on 02 September 2026

https://doi.org/10.1021/acsestwater.4c00877
ACS EST Water 2024, 4, 5913−5924

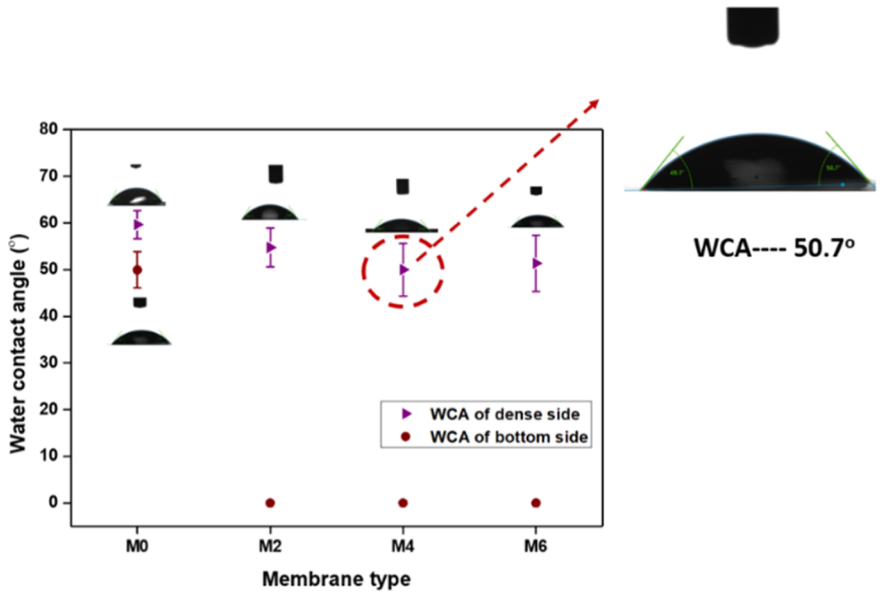


Figure 2. Water CA values for different membrane substrates (M0, M2, M4, and M6).

solution, potentially hampering the mobility of polymer chains during phase separation (the viscosity for different membrane substrates can be referred to in Figure S7). This, in turn, could yield a nonuniform membrane structure.

As per Figure 1, the improper merging of the PES molecular chains forms the top surface of a PES membrane. The top surface images displayed minimal variation across all substrates, characterized by dense surface morphologies with sparse small pores. Across a unit area of the membrane surface, the size of visible pores decreases with increasing PEOx dosages (the pores are of insufficient size to be distinguished). The average pore size analysis, based on the Guerout−Elford−Ferry equation, indicates that the surface pore size decreases for the membrane that has been modified in comparison to the pristine PES membrane substrates. The membrane pore size decreases from 56 nm for pristine PES to 48.4 nm for M4, as demonstrated in Table S2. The reduction in the pore size at the dense side of the membrane substrate can be attributed to the formation of the compact polymer network. This is due to the higher polymer concentration at the top side which reduces the free volume for pore formation. Additionally, every substrate exhibited porous morphology for the bottom side in contrast to the top side. The enhanced phase separation allows sufficient exchange of the solvent and nonsolvent. This results in the development of a more porous bottom microstructure.

Previous studies and the literature have shown that membranes typically experience shrinkage.[37,38] Our own observations align with this trend, as evidenced by a 40% reduction in thickness observed for pristine PES membranes, resulting in a thickness of 144 μm (refer to Table S2). Although the precise mechanism driving this shrinkage remains unclear, it is hypothesized that contraction of the polymer-rich phase following phase separation may be a contributing factor, pulling the polymer chains together toward the bulk of the membrane.[39] Contrarily, the addition of PEOx and goethite to the membrane led to an increase in thickness. Notably, membranes labeled M2, M4, and M6 exhibited 20−30% shrinkage. This phenomenon can be ascribed to the hydrophilic properties of PEOx and goethite, which enhance the compatibility between the nonsolvent and polymer, facilitating a more uniform phase separation process and ultimately resulting in decreased overall membrane shrinkage.

3.1.2. Water CA Analysis of the Substrates. CA analysis was applied to evaluate the contribution of PEOx and Goe NPs to the wettability of substrates. As mentioned in Figure 2, the composite substrates integrating PEOx and goethite are desirable for better wettability than pristine PES. The increased wettability is attributed to the combined presence of hydrophilic carbonyl of amide and repetitive oxazoline units within PEOx (as supported by FTIR analysis). Additionally, the hydroxyl groups present in goethite further contributed toward wettability enhancement.

It is notable that the PES substrate without any additives exhibits an identical CA value on both sides, as demonstrated in Figure 2. However, the membrane substrate incorporating PEOx and goethite achieved superhydrophilicity on the bottom or the loose side of the membrane. This can be attributed to the presence of C(O)−N of PEOx providing plenty of hydrogen bonding sites. Furthermore, a decline in the water CA was also detected on the top or dense side of these membrane substrates. This may be due to the migration of Goe NPs toward the dense side of the surface, hence contributing toward the enhanced hydrophilicity of the dense side. This migration was visually observed as a slight change in the surface color to a brown shade on the dense side of the membrane. Due to this distribution of PEOx and Goe NPs, we were able to create substrates having a hydrophilic dense side and super hydrophilic loose side.

3.1.3. Porosity of the Substrates. Elevated porosity corresponds to a decreased hydraulic resistance within the membrane, indicative of elevated hydraulic permeability. The porosity analysis of our study reveals a correlation between the increasing PEOx dosage and elevated porosity levels. The porosity of the pristine PES membrane (M0), measuring 49.25%, demonstrated a notable enhancement to 85% for (M4) with a 4 wt % PEOx dosage, refer to Figure 3. These findings are supported by the SEM images. Subsequent increase in PEOx dosage beyond 4 wt % did not show a significant enhancement in porosity. It is observed that higher

https://doi.org/10.1021/acsestwater.4c00877
ACS EST Water 2024, 4, 5913−5924

Downloaded from pubs.acs.org/aewcaa/article-pdf/4/12/5913/3163023/ew4c00877.pdf by DOKUZ EYLUL UNIV user on 02 September 2026

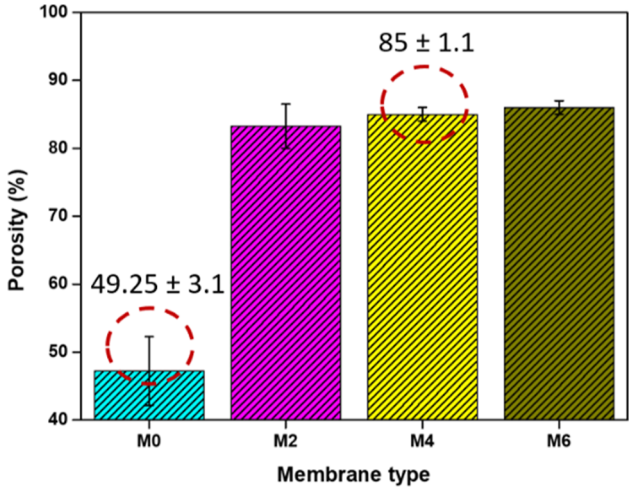


Figure 3. Porosity values for different membrane substrates (M0, M2, M4, and M6).

porosity is primarily the major aspect contributing to a smaller structural parameter value for the substrate, hence leading toward the reduced value of ICP during the FO process.[31] Hence, the substrates modified with PEOx and goethite can result in a reduced structural parameter and improved ICP.

3.1.4. XRD and FTIR Evaluation. The utilization of FTIR and XRD characterization techniques was employed to determine the presence of PEOx and Goe NPs within the membrane substrates. While the observed increase in membrane porosity and decrease in CA values indicate PEOx and goethite effects, FTIR and XRD analyses provide deeper insights into their interaction within the membrane substrate and their characteristics. FTIR analysis confirms the presence of PES and PEOx, refer to Figure 4. The strong peak of the C_6H_6 benzene ring stretch at 1587 cm^{-1} confirms the aromatic band of polyether sulfone.[40] The peak at 1476 cm^{-1} is related to the representative peak of the C−S stretch. The peaks at 1101 cm^{-1}, 1149 cm^{-1}, and 1239 cm^{-1} relate to C−O, O═S═O, and C−O−C of PES.[41] The peak occurring at 1637 cm^{-1} defines the presence of C═O of the primary amide group, and the peak at 3493 cm^{-1} is related to the NH stretching, confirming the presence of PEOx in substrates modified by PEOx and Goe NPs.[42,43] The peaks related to the Goe NPs are not confirmed by FTIR. This may be credited to the lower percentage of NPs used with respect to polymer concentrations in the membrane substrate preparation. Besides FTIR, an XRD investigation was conducted to identify the characteristic peaks associated with the additives incorporated into the membrane substrate. Figure 4 illustrates that the membrane substrates prepared by incorporating the PEOx and Goe NPs exhibit additional peaks in contrast to those of the pristine PES membrane substrates. Specifically, the XRD spectra of the membrane substrate containing Goe NPs displayed distinct peaks at 21.40, 33.53, 34.8, and 36.73°, indicative of the presence of the Goe NPs. These findings align well with the data cited in the literature for goethite, with all observed reflections validating the presence of goethite.[44,45] Additionally, the sharp peak observed at 20° corresponds to PES.[46]

3.2. Properties and Microstructure of the Active Layer. The IP between the MPD and TMC solution facilitated the creation of a polyamide layer on the membrane substrates. SEM analysis, as illustrated in Figure 5, confirms the occurrence of the polyamide layer on the surface of the membrane substrates. Although there are some disparities between the pristine PES and PES substrates modified with PEOx and goethite, the surface of pristine PES unveiled a grassy-kind structure with an open surface with a typical ridge and valley structure that was observed for the M0 membrane. This can be due to the presence of a larger pore size on the

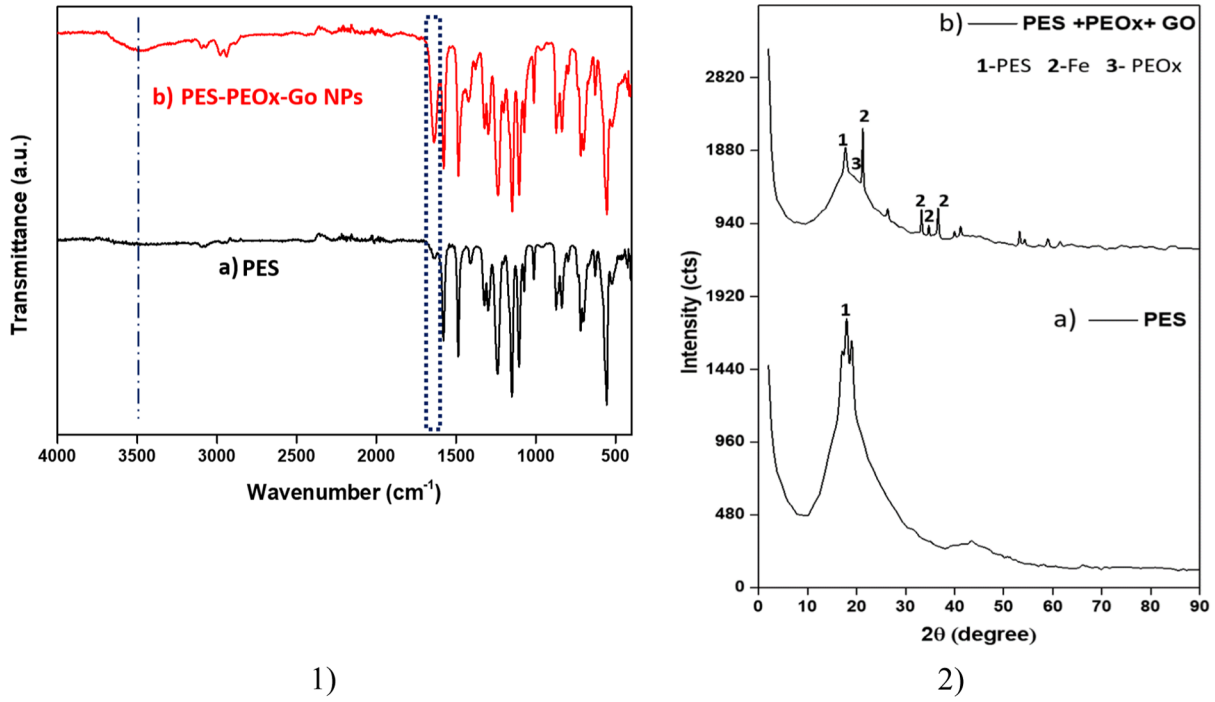


Figure 4. Represents (1) comparison of FTIR spectra for the (1a) pristine PES membrane and (1b) membrane substrate having PES/PEOx/Goe NPs and (2) XRD characterization of the membrane substrate sample for (2a) pristine PES and (2b) membrane containing PES/PEOx/Goe NPs.

Downloaded from pubs.acs.org/aewcaa/article-pdf/4/12/5913/3163023/ew4c00877.pdf by DOKUZ EYLUL UNIV user on 02 September 2026

https://doi.org/10.1021/acsestwater.4c00877
ACS EST Water 2024, 4, 5913−5924

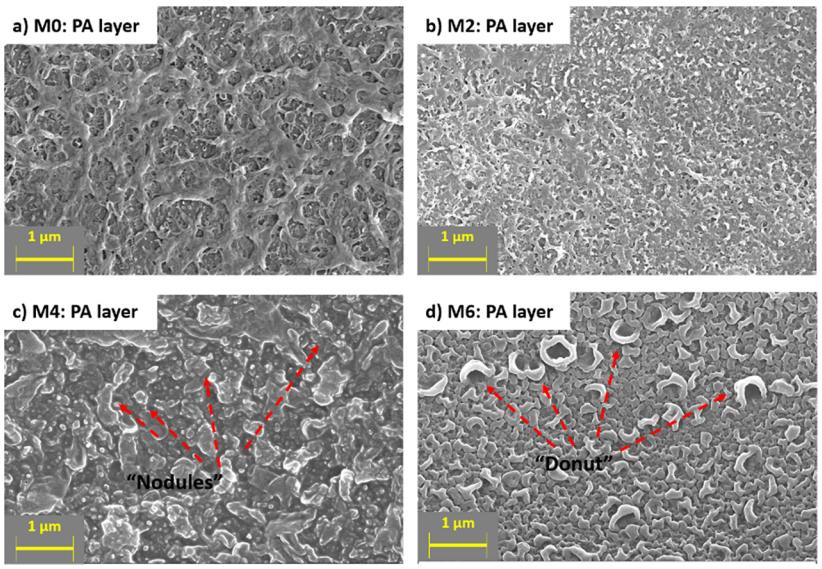


Figure 5. FESEM images taken at 20 KX magnification representing the polyamide layer prepared over (a) M0, (b) M2, (c) M4, and (d) M6 membrane substrates.

Table 2. Intrinsic Properties Related to the TFC Membranes

	A				
membranes	LMH/bar	$\times 10^{-12}$ m/s Pa	*R* (%)	*B* ($\times 10^{-7}$ m/s)	*S* (mm)
TFC-M0	2.42 ± 0.29	6.72 ± 0.8	89	0.745 ± 0.08	12.57 ± 0.31
TFC-M2	2.80 ± 0.20	7.77 ± 0.55	90	0.76 ± 0.06	8.3 ± 0.11
TFC-M4	2.84 ± 0.25	7.8 ± 0.78	91	0.86 ± 0.09	3.9 ± 0.08
TFC-M6	2.74 ± 0.07	7.55 ± 0.25	91	0.61 ± 0.02	5.496 ± 0.035

membrane surface. In contrast, the top surface of the modified substrates has distinct structures. The M4 membrane type exhibits small nodules (as marked by red dotted lines) along with some leaf-like structures due to the enhanced hydrophilic membrane substrate. The nodules seem more prominent for the M4 membrane, and some of the nodules become donut-shaped for the M6 substrate. This can be due to the expulsion of carbon dioxide gas molecules from the surface.

The difference in the microstructure of the polyamide active layer is due to the MPD molecules that migrated on the membrane substrates via convection and diffusion. This convection helps to develop the diverse morphologies over the membrane substrates.[47] It has been observed that Marangoni convection plays a crucial role in the creation of such a morphology during the preparation of the polyamide layer. The Marangoni convection helps to develop a turbulent flow resulting in twisting and bending of the preformed polyamide layer. Also, a more hydrophilic substrate leads to the formation of a smooth polyamide layer in comparison to the hydrophobic surface, which favors rapid transfer of mass and hence forms a rough rejection layer.

3.3. Intrinsic Properties Pertaining to the TFC FO Membranes. Table 2 shows the transport properties of the TFC FO membranes. An augmentation can be observed in the A values after the introduction of PEOx and goethite. The value of A for TFC-M0 reaches 2.42 LMH/bar, and the A values related to TFC-M2 and TFC-M4 reach up to 2.84 LMH/bar, hence showing an improvement of 20% in the A values. The upsurge in the A value for the TFC membranes can be linked to the porous substrates observed in TFC-M2 and TFC-M4 membranes, as confirmed by SEM cross section morphologies (see Figure 1). The irregularities in the cross section of the TFC-M6 membrane substrate resulted in decreased A values for the TFC-M6 membrane. Therefore, the PEOx and Goe NPs substantially enhanced the overall performance of the TFC membranes with regard to the A value. The NaCl rejection rate R shows a change from 88% for the TFC-M0 membrane to 91% for the TFC-M4 membrane. The increase in the value of salt rejection for TFC-M4 is due to the formation of a better rejection layer, in contrast to TFC-M0. However, the *R* values still remain good and showed less fluctuation for all of the TFC membrane substrates. The salt permeability B achieved in our study shows an increase in value from 0.745 for the TFC-M0 membrane to 0.86 for the TFC-M4 membrane. A slight increase in the B value for TFC-M4 is noticeable due to the increased value of A for the TFC-M4 membrane.

Structure parameter "*S*" is an essential variable to determine the suitability of the TFC membrane. This parameter can be described as the diffusion distance that needs to be crossed by the solute particles to pass through the substrate layer. This is also a parameter that helps to estimate the ICP in the process. Usually, a lesser value of *S* shows a lower ICP. As mentioned in Table 2, the value of S for the TFC-M0 membrane exhibits a higher value of 12.57 mm, indicating that pristine PES cannot be suitable for efficient TFC FO membranes. The results indicated that the addition of PEOx and Goe NPs exhibited a reduction in the structural parameter. The value of S was reduced to 3.9 mm for the TFC-M4 membrane, appropriate for application in the FO process. The intrinsic properties pertaining to the *S* parameter of TFC membranes are given in Table S3.

https://doi.org/10.1021/acsestwater.4c00877
ACS EST Water 2024, 4, 5913−5924

Downloaded from pubs.acs.org/aewcaa/article-pdf/4/12/5913/3163023/ew4c00877.pdf by DOKUZ EYLUL UNIV user on 02 September 2026

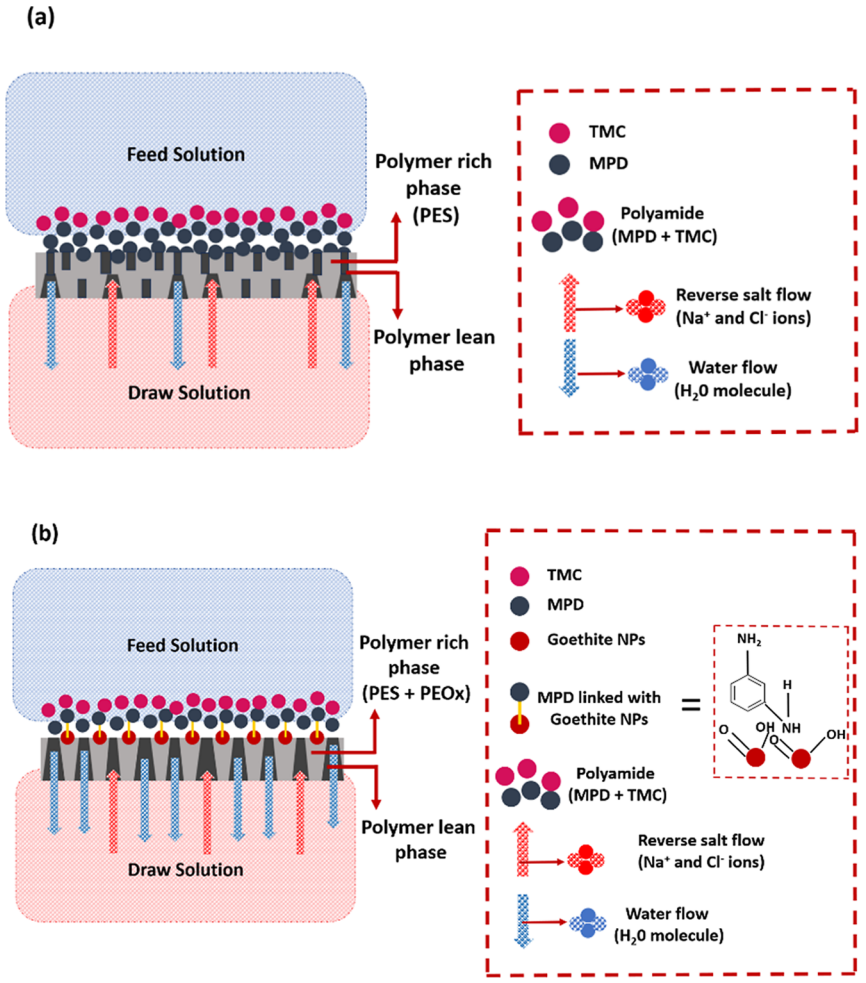


Figure 6. (a) Mechanism related to the development of TFC membrane prepared from pristine PES and (b) mechanism related to the development of TFC membrane modified with PEOx and goethite.

3.4. Insight to the Mechanism. Utilizing pristine PES for fabricating the membrane support layer generally results in membranes with macro-voids throughout most sections and a thin finger-like layer near the top surface. Although the majority of the section of pristine PES lacks the interconnectedness of the pores, as demonstrated in Figure 6a, finger-like morphologies with better interconnectedness are a prerequisite to provide flow channels for the transport of water. The introduction of PEOx with PES as an additive markedly enhances the diffusion rate during the phase separation process. This is due to the hydrophilic characteristic of PEOx, which helps in increasing thermodynamic instability and facilitating a more efficient exchange between the DMAc as solvent and water as nonsolvent.[48] This helps in the formation of flow channels across the membrane cross section, hence contributing toward improved water permeability, enhanced porosity, and reduced water flow resistance (refer to the Figure 6b). In addition to this, the presence of C(O)−N bonds within the PEOx provides plenty of hydrogen bonding sites and thus helps in achieving better membrane-wetting characteristics.[49]

During phase inversion, there is a competitive diffusion between the solvent and nonsolvent, establishing a concentration gradient. This gradient acts as a thermodynamic driving force, propelling Goe NPs toward the dense skin layer. These groups enhance the surface wettability. A decrease in the WCA values of the dense side of the membrane substrate provides a hydrophilic and smoother surface for the IP reaction to take place. A hydrophilic substrate restricts the diffusion of MPD to the organic phase, resulting in a thin PA layer, hence favoring improved water permeability.

The presence of the hydroxyl group on the membrane substrate was confirmed by XPS analysis; refer to Figure S6. Figure S6 shows satellite peaks on the survey report and a small peak at a binding energy of 532 eV, confirming the presence of oxygen as hydroxide. However, the peak was not sharp enough and this can be ascribed to the low concentration of goethite utilized in comparison to the host polymers. The presence of hydroxyl groups of goethite may facilitate the adsorption of additional MPD through hydrogen bonding.[50] Refer to Figure 6b). This functionality is advantageous for the formation of a robust polyamide layer, ultimately contributing to improved membrane selectivity and performance.

Consequently, a membrane modified with PEOx and Goe NPs exhibits enhanced finger-like pore morphologies and a cross-linked polyamide layer. These structural improvements can result in higher water flux, reduced reverse salt flux, and improved structural parameters, contributing to the enhanced performance of the modified TFC FO membrane.

3.5. Functionality of the TFC FO Membranes. The diverse TFC FO membranes were evaluated to check their performances under the FO and PRO modes utilizing 2 molar

https://doi.org/10.1021/acsestwater.4c00877
ACS EST Water 2024, 4, 5913−5924

Downloaded from pubs.acs.org/aewcaa/article-pdf/4/12/5913/3163023/ew4c00877.pdf by DOKUZ EYLUL UNIV user on 02 September 2026

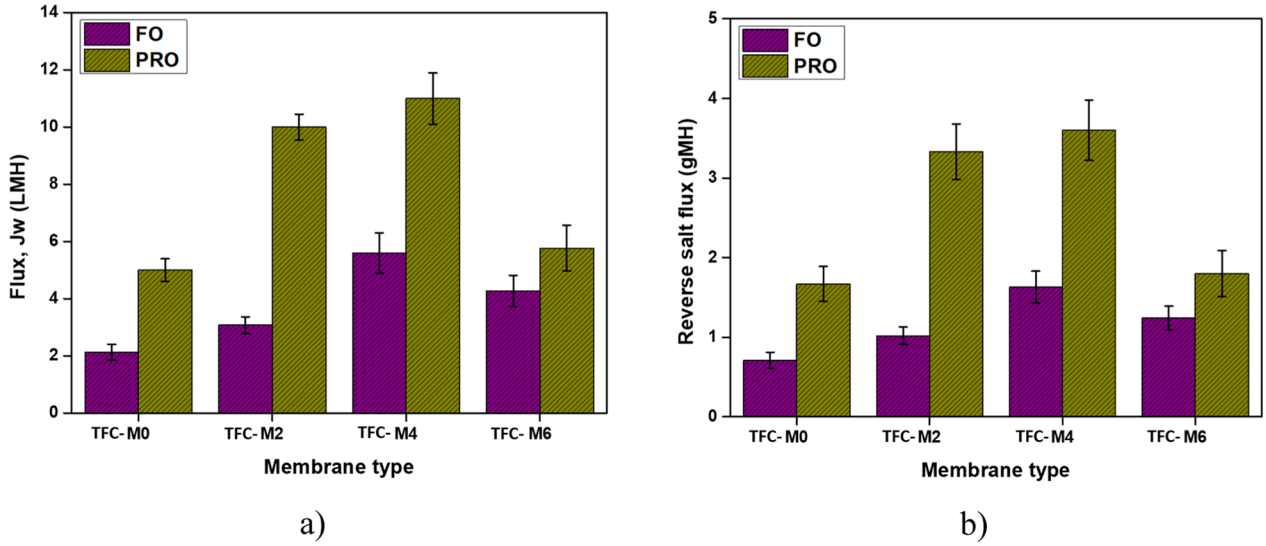


Figure 7. FO performance of different TFC FO membranes. (a) Water flux and (b) reverse salt flux. Diverse TFC membranes are represented based on the notations given for the membrane support layer.

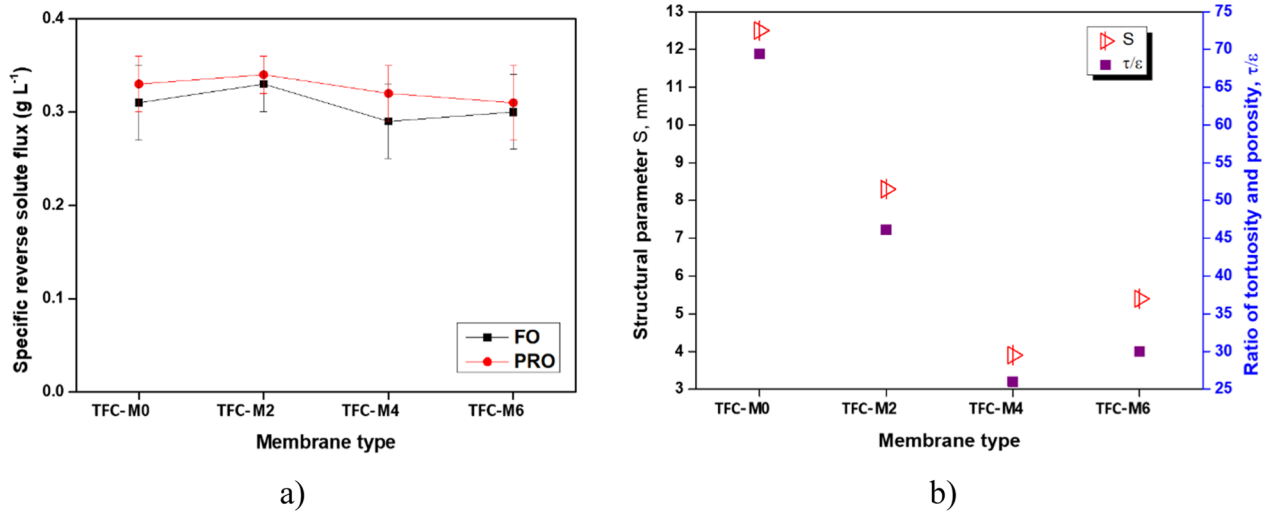


Figure 8. Represents (a) SRSF performance of different TFC FO membrane for FO and PRO modes and (b) comparison of structural parameters of different TFC membranes.

of NaCl as the draw and distilled water as the feed solutions, respectively. The values pertaining to water and reverse salt flux, along with specific salt flux, are mentioned in Figure 7. Figure 7a represents the data for water flux related to the different TFC membranes. In agreement with more prior works, a higher value of water flux was detected for all the prepared TFC membranes under the PRO mode compared to FO. This observation can be ascribed to the severe dilutive ICP, which can lessen the water flux when the membranes are operated in the FO condition. Similarly, a slight concentrative ICP arises for the PRO mode. The water fluxes significantly increased after the addition of PEOx. From Figure 7a, it can be derived that the water flux value increased significantly from 2.29 LMH for TFC-M0 to 5.62 LMH for TFC-M4 in the FO mode, and for PRO mode this changes from 5.06 LMH for TFC-M0 to 11.25 LMH for TFC-M4. This change can be accredited to the lower S value, along with the formation of flow channels obtained for the TFC-M4 membrane. This water flux value improvement was only marginal for a PEOx concentration within 4 wt %. The outcomes for the reverse salt flux for diverse modes are displayed in Figure 7b. The reverse salt fluxes enhanced somewhat from 0.71 gMH for TFC-M0 to 1.63 gMH for TFC-M4 in the FO mode, and for the PRO mode it changes from 1.67 gMH for TFC-M0 to 3.6 gMH for TFC-M4.

One specific performance metric that is used for comparing the performances of different membranes and evaluating the efficiency of the osmotic process is specific salt flux, also known as the reverse salt flux/water flux ratio. It is preferred for a membrane to have a lower specific salt flux. Figure 8a shows that the specific salt flux reduced substantially after the addition of the PEOx. The lowest value of specific salt flux occurred for the TFC-M4 membrane. This can be accredited to the greater water flux value obtained for the TFC-M4 membrane when operated in the FO and PRO modes.

Figure 8b discusses the structural parameters obtained for our TFC membranes. The analysis showed a high value of S for pristine TFC FO membrane. This can be due to lower pore density and poorly formed flow channels that occurred for pristine PES membrane. This, in turn, reduced the pure water

https://doi.org/10.1021/acsestwater.4c00877
ACS EST Water 2024, 4, 5913−5924

Downloaded from pubs.acs.org/aewcaa/article-pdf/4/12/5913/3163023/ew4c00877.pdf by DOKUZ EYLUL UNIV user on 02 September 2026

permeability and water flux obtained in the FO mode, hence leading toward a very high value of S.

However, the figure displays a decrease in the value of S after the addition of PEOx into the polymer blend. The S value decreases from 12.5 mm for the TFC-M0 membrane to 3.9 mm for the TFC-M4 membrane. This reduction in the value of S is basically due to the presence of the flow channels being formed after the addition of PEOx (as supported by the SEM images), providing the ease with which the water can flow through the membrane and hence experience lower resistance. The ratio of τ/ε, as shown in Figure 8b, also displays that the microstructure obtained for the M4 membrane substrate can be considered as optimal for the FO process.

Additionally, varying salt concentrations were used to evaluate the performance of the TFC-M0 and TFC-M4 membranes; refer to Figure S8. The data suggests an increment in the overall water flux as the concentration of the draw solution rises. Though, the water flux enhanced significantly for TFC-M4 in contrast to TFC-M0. As per the data, the water flux for the TFC-M4 membrane increased by 28%/32% from 0.5 molar NaCl to 2.0 molar NaCl draw solution for FO/PRO modes, whereas the flux of water amplified solely by 8%/10% for the TFC-M0 membrane under the same configurations. The significant difference between the water flux values obtained for TFC-M0 and TFC-M4 membranes supports the fact that the introduction of PEOx and Goe NPs could reduce ICP during the FO process.

4. CONCLUSION

In this work, a cost-effective TFC FO membrane was developed, utilizing poly(ether sulfone) as the backbone material. The membrane was augmented with PEOx and Goe NPs as hydrophilic modifiers. FTIR and XRD analyses confirm the presence of PEOx and Goe NPs within the membrane substrate. Wetting characteristics were significantly improved with the incorporation of PEOx and Goe NPs, as demonstrated by a reduction in the CA values. Moreover, porosity enhancements were observed, as supported by SEM analysis, which revealed an increase in the number of pores and the development of finger-like channels across the cross section of the membranes.

Among the various TFC FO membranes evaluated, TFC-M4 exhibited the most promising performance metrics, showcasing the lowest S parameter and superior water flux for both the FO and PRO modes. Additionally, TFC-M4 demonstrated lower values of specific salt flux compared to those of other membranes, emphasizing its potential for practical applications in desalination processes. It is important to note that the structural parameter initially remained high for the pristine PES membrane; it notably improved upon the addition of PEOx and Goe NPs. However, future endeavors may be directed toward improving the S value, thereby enhancing overall membrane performance.

■ ASSOCIATED CONTENT

Supporting Information

The Supporting Information is available free of charge at https://pubs.acs.org/doi/10.1021/acsestwater.4c00877.

Preparatory steps for preparing the support layer; AFM analysis of different substrates for determining the concentration of Goe NPs to be used; tabular form AFM results for the prepared substrates; preparatory steps for preparing the active layer; lab-scale setup of FO for testing of the membrane; EDX spectra for pristine and modified membrane substrates; XPS data representing survey report of optimized membrane; viscosity measurement; TFC membrane performance under varying strength of salt concentration; pore size, porosity, and thickness of different prepared membrane substrates; and intrinsic properties related to diverse fabricated TFC membranes (PDF)

■ AUTHOR INFORMATION

Corresponding Author

Bhaskar Jyoti Deka − *Advanced Membrane Research Lab, Department of Hydrology, Indian Institute of Technology Roorkee, Haridwar, Uttarakhand 247667, India; Centre for Nanotechnology, Indian Institute of Technology Roorkee, Haridwar, Uttarakhand 247667, India;* orcid.org/0000-0002-4199-4713; Email: bhaskar.deka@hy.iitr.ac.in

Author

Shubham Ketan Sharma − *Advanced Membrane Research Lab, Department of Hydrology, Indian Institute of Technology Roorkee, Haridwar, Uttarakhand 247667, India;* orcid.org/0009-0008-6234-9255

Complete contact information is available at: https://pubs.acs.org/10.1021/acsestwater.4c00877

Author Contributions

CRediT: **Shubham Ketan Sharma** conceptualization, formal analysis, investigation, methodology, validation, visualization, writing - original draft, writing - review & editing; **Bhaskar Jyoti Deka** conceptualization, funding acquisition, investigation, methodology, project administration, resources, supervision, validation, visualization, writing - review & editing.

Funding

The primary funding was received from the Faculty Initiation Grant, Sponsored Research and Industrial Consultancy (HYD/FIG/100906), and Technology Readiness Level Booster (TRL-2129-HYD/23−24) from Indian Institute of Technology Roorkee, India. Additional support was provided from the grant received under project from the Indian Space Research Organisation (STC-1941-HYD), India awarded to Dr. Bhaskar Jyoti Deka. This research was also supported by the Ministry of Human Resource Development, Government of India, through a doctoral scholarship awarded to the first author.

Notes

The authors declare no competing financial interest.

The process (Application No. 202311057602) and product (Application No. 202311057597) have been submitted for patent registration under the Indian Patent Act.

■ ACKNOWLEDGMENTS

The authors would like to extend their sincere gratitude to the Department of Hydrology, Institute Instrumentation Centre, Indian Institute of Technology Roorkee, and Centre for Nanotechnology, Indian Institute of Technology Roorkee, for providing the necessary support and facilities throughout this research.

■ REFERENCES

(1) McDonald, R. I.; Weber, K.; Padowski, J.; Flörke, M.; Schneider, C.; Green, P. A.; Gleeson, T.; Eckman, S.; Lehner, B.; Balk, D.;

Downloaded from pubs.acs.org/aewcaa/article-pdf/4/12/5913/3163023/ew4c00877.pdf by DOKUZ EYLUL UNIV user on 02 September 2026

Boucher, T.; Grill, G.; Montgomery, M. Water on an Urban Planet: Urbanization and the Reach of Urban Water Infrastructure. *Global Environ. Change* **2014**, *27* (1), 96−105.
(2) Sharma, S. K.; Truong, D. Q.; Guo, J.; An, A. K.; Naidu, G.; Deka, B. J. Recovery of Rubidium from Brine Sources Utilizing Diverse Separation Technologies. *Desalination* **2023**, *556*, 116578.
(3) Chekli, L.; Phuntsho, S.; Kim, J. E.; Kim, J.; Choi, J. Y.; Choi, J. S.; Kim, S.; Kim, J. H.; Hong, S.; Sohn, J.; Shon, H. K. A Comprehensive Review of Hybrid Forward Osmosis Systems: Performance, Applications and Future Prospects. *J. Membr. Sci.* **2016**, *497*, 430−449.
(4) Farahbakhsh, J.; Golgoli, M.; Khiadani, M.; Najafi, M.; Suwaileh, W.; Razmjou, A.; Zargar, M. Recent Advances in Surface Tailoring of Thin Film Forward Osmosis Membranes: A Review. *Chemosphere* **2024**, *346* (February2023), 140493.
(5) Qasim, M.; Darwish, N. A.; Sarp, S.; Hilal, N. Water Desalination by Forward (Direct) Osmosis Phenomenon: A Comprehensive Review. *Desalination* **2015**, *374*, 47−69.
(6) Li, D.; Yan, Y.; Wang, H. Recent Advances in Polymer and Polymer Composite Membranes for Reverse and Forward Osmosis Processes. *Prog. Polym. Sci.* **2016**, *61*, 104−155.
(7) Wang, Y.; Ou, R.; Wang, H.; Xu, T. Graphene Oxide Modified Graphitic Carbon Nitride as a Modifier for Thin Film Composite Forward Osmosis Membrane. *J. Membr. Sci.* **2015**, *475*, 281−289.
(8) Shen, L.; Xiong, S.; Wang, Y. Graphene Oxide Incorporated Thin-Film Composite Membranes for Forward Osmosis Applications. *Chem. Eng. Sci.* **2016**, *143*, 194−205.
(9) Duong, P. H. H.; Chisca, S.; Hong, P. Y.; Cheng, H.; Nunes, S. P.; Chung, T. S. Hydroxyl Functionalized Polytriazole-Co-Polyoxadiazole as Substrates for Forward Osmosis Membranes. *ACS Appl. Mater. Interfaces* **2015**, *7* (7), 3960−3973.
(10) Zhao, S.; Sun, N.; Dou, P.; Lin, S.; He, T. Structure Parameter as an Intrinsic Property of Thin-Film Composite Forward Osmosis Membrane. *Desalination* **2024**, *581* (April), 117616.
(11) Kanagaraj, P.; Shanmugaraja, M.; Rana, D.; Sureshkumar, M.; Mahendraprabhu, K. M. A.; Mohamed, I.; Venkatesan, R.; Al-Kahtani, A. A. Development of High Performance Thin-Film (Nano) Composite Membranes for Forward Osmosis Desalination Applications- a Review. *Mater. Sci. Eng. B* **2024**, *299*, 116966.
(12) Flanagan, M. F.; Escobar, I. C. Novel Charged and Hydrophilized Polybenzimidazole (PBI) Membranes for Forward Osmosis. *J. Membr. Sci.* **2013**, *434*, 85−92.
(13) Chen, G. E.; Sun, W. G.; Wu, Q.; Kong, Y. F.; Xu, Z. L.; Xu, S. J.; Zheng, X. P. Effect of Cellulose Triacetate Membrane Thickness on Forward-Osmosis Performance and Application for Spent Electroless Nickel Plating Baths. *J. Appl. Polym. Sci.* **2017**, *134* (28), 1−10.
(14) Zhang, B.; Zou, W.; Wu, P.; Zhang, J.; Kong, W.; Chen, X.; Wu, C.; Wang, Y. Carbon Dots Regulating Microstructure of Polyamide Layer of Forward Osmosis Membrane for Anti-Biofouling and Unexpected Dual-Enhancement in Water Flux and Salt Rejection. *Sustainable Mater. Technol.* **2024**, *40* (February), No. e00910.
(15) Kwon, S. B.; Lee, J. S.; Kwon, S. J.; Yun, S. T.; Lee, S.; Lee, J. H. Molecular Layer-by-Layer Assembled Forward Osmosis Membranes. *J. Membr. Sci.* **2015**, *488*, 111−120.
(16) Sun, Z.; Zhang, S.; Zhang, Z.; Yang, Y.; Zhang, C.; Qian, Y.; Ren, X. A Novel Antifouling Polyamide Thin-Film Composite Forward Osmosis Membrane Fabricated by Poly(m-Phenylene Isophthalamide) for Seawater Desalination. *J. Environ. Chem. Eng.* **2023**, *11* (5), 110739.
(17) Zhou, Z.; Lee, J. Y.; Chung, T. S. Thin Film Composite Forward-Osmosis Membranes with Enhanced Internal Osmotic Pressure for Internal Concentration Polarization Reduction. *Chem. Eng. J.* **2014**, *249*, 236−245.
(18) Wang, Y.; Zhang, M.; Liu, Y.; Xiao, Q.; Xu, S. Quantitative Evaluation of Concentration Polarization under Different Operating Conditions for Forward Osmosis Process. *Desalination* **2016**, *398*, 106−113.
(19) Shokrollahzadeh, S.; Tajik, S. Fabrication of Thin Film Composite Forward Osmosis Membrane Using Electrospun Polysulfone/Polyacrylonitrile Blend Nanofibers as Porous Substrate. *Desalination* **2018**, *425* (May 2017), 68−76.
(20) Yu, Y.; Seo, S.; Kim, I. C.; Lee, S. Nanoporous Polyethersulfone (PES) Membrane with Enhanced Flux Applied in Forward Osmosis Process. *J. Membr. Sci.* **2011**, *375* (1−2), 63−68.
(21) Kallem, P.; Gaur, R.; Pandey, R. P.; Hasan, S. W.; Choi, H.; Banat, F. Thin Film Composite Forward Osmosis Membranes Based on Thermally Treated PAN Hydrophilized PVDF Electrospun Nanofiber Substrates for Improved Performance. *J. Environ. Chem. Eng.* **2021**, *9* (5), 106240.
(22) Bagherzadeh, M.; Nikkhoo, M.; Mahdi, M. Journal of Environmental Chemical Engineering Polyethersulfone/Polyamide Thin-Film Nanocomposite Membrane Decorated by WS 2 -Cys-UiO-66- (CO 2 H) 2 Nanocomposites for Forward Osmosis. *J. Environ. Chem. Eng.* **2023**, *11* (3), 109959.
(23) Sirinupong, T.; Youravong, W.; Tirawat, D.; Lau, W. J.; Lai, G. S.; Ismail, A. F. Synthesis and Characterization of Thin Film Composite Membranes Made of PSF-TiO2/GO Nanocomposite Substrate for Forward Osmosis Applications. *Arab. J. Chem.* **2018**, *11* (7), 1144−1153.
(24) Sahebi, S.; Phuntsho, S.; Woo, Y. C.; Park, M. J.; Tijing, L. D.; Hong, S.; Shon, H. K. Effect of Sulphonated Polyethersulfone Substrate for Thin Film Composite Forward Osmosis Membrane. *Desalination* **2016**, *389*, 129−136.
(25) VillanoKommedal, L. D. R.; Fijten, M. W. M.; Schubert, U. S.; Hoogenboom, R.; Kelland, M. A.; Kelland, M. A. A Study of the Kinetic Hydrate Inhibitor Performance and Seawater Biodegradability of a Series of Poly(2-Alkyl-2-Oxazoline)s. *Energy Fuels* **2009**, *23* (7), 3665−3673.
(26) Aliakbarzadeh, S.; Abdouss, M.; Ali, H.; Rahdar, A. Gelatin Methacrylate/Poly (2-Ethyl-2-Oxazoline) Porous Hydrogel Loaded with Kartogenin Drug as a Biocompatible Scaffold for Cartilage Tissue Regeneration. *J. Mol. Liq.* **2024**, *404* (May), 124982.
(27) Hsiue, G. H.; Wang, C. H.; Lo, C. L.; Wang, C. H.; Li, J. P.; Yang, J. L. Environmental-Sensitive Micelles Based on Poly(2-Ethyl-2-Oxazoline)-b-Poly(l-Lactide) Diblock Copolymer for Application in Drug Delivery. *Int. J. Pharm.* **2006**, *317* (1), 69−75.
(28) Lin, P.; Clash, C.; Pearce, E. M.; Kwei, T. K.; Aponte, M. A. Solubility and Miscibility of Poly(Ethyl Oxazoline). *J. Polym. Sci. B Polym. Phys.* **1988**, *26* (3), 603−619.
(29) Zhang, L.; Chae, S. R.; Lin, S.; Wiesner, M. R. Proton-Conducting Composite Membranes Derived from Ferroxane-Polyvinyl Alcohol Complex. *Environ. Eng. Sci.* **2012**, *29* (2), 124−132.
(30) Saniei, N.; Ghasemi, N.; Zinatizadeh, A. A.; Zinadini, S.; Ramezani, M.; Derakhshan, A. A. Preparation and Characterization of a Novel Antifouling Nano Filtration Poly Ethersulfone (PES) Membrane by Embedding Goethite-Tannic Acid Nanoparticles. *Sep. Purif. Technol.* **2020**, *241* (February), 116646.
(31) Emadzadeh, D.; Lau, W. J.; Matsuura, T.; Rahbari-Sisakht, M.; Ismail, A. F. A Novel Thin Film Composite Forward Osmosis Membrane Prepared from PSf-TiO2 Nanocomposite Substrate for Water Desalination. *Chem. Eng. J.* **2014**, *237*, 70−80.
(32) Liu, X.; Ng, H. Y. Fabrication of Layered Silica-Polysulfone Mixed Matrix Substrate Membrane for Enhancing Performance of Thin-Film Composite Forward Osmosis Membrane. *J. Membr. Sci.* **2015**, *481*, 148−163.
(33) Wijmans, J. G.; Kant, J.; Mulder, M. H. V.; Smolders, C. A. Phase Separation Phenomena in Solutions of Polysulfone in Mixtures of a Solvent and a Nonsolvent: Relationship with Membrane Formation. *Polymer* **1985**, *26* (10), 1539−1545.
(34) Hasheminasab, S.; Barzin, J.; Dehghan, R. High-Performance Hemodialysis Membrane: Influence of Polyethylene Glycol and Polyvinylpyrrolidone in the Polyethersulfone Membrane. *J. Membr. Sci. Res.* **2020**, *6* (4), 438−448.
(35) Smolders, C. A.; Reuvers, A. J.; Boom, R. M.; Wienk, I. M. Microstructures in Phase-Inversion Membranes. Part 1. Formation of Macrovoids. *J. Membr. Sci.* **1992**, *73* (2−3), 259−275.

Downloaded from pubs.acs.org/aewcaa/article-pdf/4/12/5913/3163023/ew4c00877.pdf by DOKUZ EYLUL UNIV user on 02 September 2026

https://doi.org/10.1021/acsestwater.4c00877
ACS EST Water 2024, 4, 5913−5924

(36) Wang, D. M.; Lin, F. C.; Wu, T. T.; Lai, J. Y. Formation Mechanism of the Macrovoids Induced by Surfactant Additives. *J. Membr. Sci.* **1998**, *142* (2), 191−204.
(37) Menut, P.; Su, Y. S.; Chinpa, W.; Pochat-Bohatier, C.; Deratani, A.; Wang, D. M.; Huguet, P.; Kuo, C. Y.; Lai, J. Y.; Dupuy, C. A Top Surface Liquid Layer during Membrane Formation Using Vapor-Induced Phase Separation (VIPS)-Evidence and Mechanism of Formation. *J. Membr. Sci.* **2008**, *310* (1−2), 278−288.
(38) Tweddle, T. A.; Kutowy, O.; Thayer, W. L.; Sourirajan, S. Polysulfone Ultrafiltration Membranes. *Ind. Eng. Chem. Prod. Res. Dev.* **1983**, *22* (2), 320−326.
(39) Sadrzadeh, M.; Bhattacharjee, S. Rational Design of Phase Inversion Membranes by Tailoring Thermodynamics and Kinetics of Casting Solution Using Polymer Additives. *J. Membr. Sci.* **2013**, *441*, 31−44.
(40) Alvi, M. A. U. R.; Khalid, M. W.; Ahmad, N. M.; Niazi, M. B. K.; Anwar, M. N.; Batool, M.; Cheema, W.; Rafiq, S. Polymer Concentration and Solvent Variation Correlation with the Morphology and Water Filtration Analysis of Polyether Sulfone Microfiltration Membrane. *Adv. Polym. Technol.* **2019**, *2019*, 1−11.
(41) Hosseini, S. S.; Torbati, S. F.; Shahmirzadi, M. A. A.; Tavangar, T. Fabrication, Characterization, and Performance Evaluation of Polyethersulfone/TiO2 Nanocomposite Ultrafiltration Membranes for Produced Water Treatment. *Polym. Adv. Technol.* **2018**, *29* (10), 2619−2631.
(42) Tehrani, A. D.; Neysi, E. Surface Modification of Cellulose Nanowhisker throughout Graft Polymerization of 2-Ethyl-2-Oxazoline. *Carbohydr. Polym.* **2013**, *97* (1), 98−104.
(43) Yang, J.; Li, L.; Ma, C.; Ye, X. Degradable Polyurethane with Poly(2-Ethyl-2-Oxazoline) Brushes for Protein Resistance. *RSC Adv.* **2016**, *6* (74), 69930−69938.
(44) Wang, B.; Wu, H.; Yu, L.; Xu, R.; Lim, T. T.; David Lou, X. W. Template-Free Formation of Uniform Urchin-like α-FeOOH Hollow Spheres with Superior Capability for Water Treatment. *Adv. Mater.* **2012**, *24* (8), 1111−1116.
(45) Jaiswal, A.; Banerjee, S.; Mani, R.; Chattopadhyaya, M. C. Synthesis, Characterization and Application of Goethite Mineral as an Adsorbent. *J. Environ. Chem. Eng.* **2013**, *1* (3), 281−289.
(46) Khayet, M.; García-Payo, M. C. X-Ray Diffraction Study of Polyethersulfone Polymer, Flat-Sheet and Hollow Fibers Prepared from the Same under Different Gas-Gaps. *Desalination* **2009**, *245* (1−3), 494−500.
(47) Li, X.; Wang, K. Y.; Helmer, B.; Chung, T. S. Thin-Film Composite Membranes and Formation Mechanism of Thin-Film Layers on Hydrophilic Cellulose Acetate Propionate Substrates for Forward Osmosis Processes. *Ind. Eng. Chem. Res.* **2012**, *51* (30), 10039−10050.
(48) Lorson, T.; Lübtow, M. M.; Wegener, E.; Haider, M. S.; Borova, S.; Nahm, D.; Jordan, R.; Sokolski-papkov, M.; Kabanov, A. V.; Luxenhofer, R. Biomaterials Poly (2-Oxazoline) s Based Biomaterials: A Comprehensive and Critical Update. *Biomaterials* **2018**, *178*, 204−280.
(49) Gubarev, A. S.; Lezov, A. A.; Podsevalnikova, A. N.; Mikusheva, N. G.; Fetin, P. A.; Zorin, I. M.; Aseyev, V. O.; Sedlacek, O.; Hoogenboom, R.; Tsvetkov, N. V. Conformational Parameters and Hydrodynamic Behavior of Poly (2-Methyl-2-Oxazoline) in a Broad Molar Mass Range. *Polymers* **2023**, *15*, 623.
(50) Iqubal, M.; Sharma, R.; Jheeta, S.; Kamaluddin. Thermal Condensation of Glycine and Alanine on Metal Ferrite Surface: Primitive Peptide Bond Formation Scenario. *Life* **2017**, *7*, 15.

Downloaded from pubs.acs.org/aewcaa/article-pdf/4/12/5913/3163023/ew4c00877.pdf by DOKUZ EYLUL UNIV user on 02 September 2026

https://doi.org/10.1021/acsestwater.4c00877
ACS EST Water 2024, 4, 5913−5924